Journal of Colloid and Interface Science 555 (2019) 548–557

Contents lists available at ScienceDirect

Journal of Colloid and Interface Science

journal homepage: www.elsevier.com/locate/jcis

Regular Article

Tuning the ZnO-activated carbon interaction through nitrogen modification for enhancing the H_2S removal capacity

Chao Yang [a], Song Yang [b], Huiling Fan [a,*], Yeshuang Wang [a], Ju Shangguan [a]

[a] State Key Laboratory of Coal Science and Technology, Co-founded by Shanxi Province and the Ministry of Science and Technology, Taiyuan University of Technology, West Yingze Street Number 79, Taiyuan 030024, People's Republic of China
[b] Department of Chemical Engineering, Taiyuan University of Technology, West Yingze Street Number 79, Taiyuan 030024, People's Republic of China

GRAPHICAL ABSTRACT

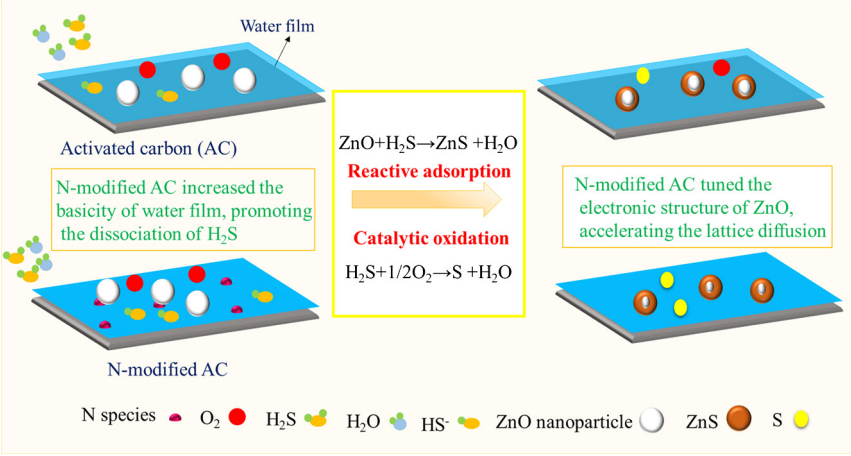

ARTICLE INFO

Article history:
Received 10 June 2019
Revised 25 July 2019
Accepted 4 August 2019
Available online 5 August 2019

Keywords:
N-modified activated carbon
Soft nitriding
Support
ZnO
H_2S removal

ABSTRACT

Herein, an unusual strategy is reported to enhance the H_2S uptake capacity by varying the ZnO-support interaction and controlling the acid-basic environment of the pore channel; this is in place of the generally reported method of decreasing ZnO nanoparticle size and optimizing their porosity. With this regard, coal based activated carbon (AC) is selected as the support and the interaction with ZnO is tuned by introducing N species on AC surface through a soft nitriding strategy. Our strategy is confirmed to be prospective based on the fact that the *N*-modifying AC supported ZnO adsorbent show a maximum breakthrough sulfur capacity (BSC) of 62.5 mg S/g sorbent, two times larger than that without *N*-modification (30.5 mg S/g sorbent). The enhanced BSC is attributed to the introduced N species, which not only increases the basicity of the water film condensed in the pores, promoting the dissociation of H_2S and H_2O, but also influences the electronic structure of ZnO, accelerating the rate of lattice diffusion during in sulfidation process. It is also found that the high BSC of sorbent with N modification is related to the doped N concentrations, ZnO dispersion and the material porosity. This paper provides a new insight for designing supported ZnO based adsorbents.

* Corresponding author.
E-mail address: fanhuiling@tyut.edu.cn (H. Fan).

https://doi.org/10.1016/j.jcis.2019.08.014
0021-9797/

1. Introduction

Hydrogen sulfide (H_2S) is a toxic contaminant that is found in natural gas, syngas and coal-derived gas. The presence of H_2S causes damage to pipelines and equipment, and can also destroy the downstream catalysts. Therefore, removing H_2S from these gases is needed before further use. Metal oxides are common adsorbents for H_2S removal due to their strong affinity. Westmoreland et al. [1] thermodynamically screened various metal oxides for H_2S removal and showed that the oxides of Fe, Zn, Mn, Mo, V, Ca, Sr, Ba, Co, Cu and W could be used as desulfurizer at high temperature. Compared with high temperature desulfurization, low temperature desulfurization has the advantages of facile operation, low cost and high desulfurization precision. For instance, the recently developed rapid proton exchange membrane fuel cells need to lower the H_2S concentration to 0.1 ppm in feed gas at ambient temperature [2]. ZnO has favorable thermodynamics at room temperature and has been extensively studied as a polishing bed desulfurizer [3,4]. However, the problem of low sulfidation extent due to the kinetic limitations is still a bottleneck for industrial application.

Supporting ZnO nanoparticles onto porous material, such as mesoporous silica [4–7], activated carbon (AC) [8], graphite oxide [9], g-C_3N_4 [10] and sepiolite [11] et al., is a simple but efficient strategy to alleviate slow sulfidation kinetics. This is because the support matrix can well disperse ZnO and also prevent the agglomeration of ZnO grains, eventually resulting in a higher availability of active adsorption sites. Furthermore, their high porosity can reduce the resistant of pore diffusion. Thus evenly dispersing ZnO nanoparticles on the support while keeping their important texture properties intact is a hot topic for researchers aiming to improve the H_2S removal performance of the sorbents. For examples, Hussain et al. [12] and Li et al. [4] investigated diverse mesoporous silica materials (MCM-41, KIT-6, SBA-15, SBA-16, and MCM-48) with different physical properties being used as support; Geng et al. [13] adopted the novel melt infiltration method to prepare the ZnO-based adsorbents instead of using the impregnation method; Balsamo et al. [14,15] improved the dispersion of ZnO on AC through adding the second active component CuO, the enhanced sulfur capacity contributed to the well dispersion of metal oxides and is also related to the synergistic effect between ZnO and CuO.

Metal oxides-support interactions are very important in catalysis and have been widely studied, since the eligible interaction can remarkably improve their catalytic performance [16,17]. Similarly, this interaction is also of great significance in desulfurization. Bandosz et al. [18,19] prepared a series of metal (oxy)hydroxide-graphite oxide adsorbents for H_2S removal. They found that the interactions between active sites and the carbonaceous support (such as the formation of surface chemical heterogeneity or the formation of new chemical bonds) contributed to the enhanced sulfur removal capacity. Cimino et al. [14,15,20] supported CuO and ZnO on different supports, such as the γ-alumina and AC. The interaction between metal oxides and AC was believed to benefit for increasing the complexity of surface sulfidation while the strong interaction between active sites and γ-alumina led to a decrease in H_2S removal capacity. Also, Ullah et al. [21] explored the effect of crystallization temperature on thiophene conversion and sulfur capacity of Ni/ZnO-Al_2O_3 sorbents. The authors concluded that high crystallization temperature could lead a strong interaction between ZnO and Al_2O_3 and the formation of inactive $ZnAl_2O_4$; this dramatically decreased the reactive adsorption desulfurization performance. Clearly, the active site-support interaction is also a non-negligible factor influencing the desulfurization performance. Despite that, few endeavors have focused on this aspect were done to improve the sorbent H_2S uptake capacity. Inspired by this, a novel idea on design of ZnO based adsorbent is fabricated via tuning the ZnO-support interactions.

AC, widely being used as support, has attracted much attentions in the field of adsorption [14], catalysis [22] and supercapacitor [23] due to the advantages of large surface area, high pore volume, relatively high mechanical strength and enriched surface oxygen-containing functional groups such as hydroxides and carboxylic groups [24–26]. These fantastic characteristics motivate us to use AC as support, especially for the enriched surface oxygen-containing functional groups, which can help introduce heteroatoms that change the surface chemistry of AC, thereby achieve the aim of manipulating the ZnO-AC interactions. Dependent on its wide commercial availability in the Chinese market, the coal based AC is selected as the support in this study. Nitrogen modified AC is used as a media to tune the ZnO-AC interactions, because this modification can alter the surface electronic structure and the acidity/basicity related to the porous environment of AC which also shows great influence on H_2S removal [27–29]. However, the conventional preparation of the *N*-functionalized AC matrix is based on pyrolysis of precursors containing N species or high-temperature annealing in an NH_3 atmosphere [30,31]. The disadvantage of high energy-consumption is that it clearly cannot meet the thesis of sustainable development.

Herein, a robust but green strategy was referenced to incorporate N species on AC surface through mild annealing with urea at 300 °C, namely the soft nitriding method [22,32]. The soft nitriding method can successfully introduce N species on carbon surfaces through reacting with NH3 and HCNO generated from thermal decomposition of urea. At the basis, a series of nitrogen modifying AC supported ZnO adsorbents with different nitrogen content or/and ZnO loading content are prepared. Therein the nitrogen content attached onto AC are controlled by modulating the urea/AC weight ratio. The effects of N doped AC on their supported ZnO adsorbents for H_2S removal and the different adsorption mechanism before and after N modification are discussed in detail. This research provides new insights for designing novel supported ZnO based adsorbents.

2. Experimental

2.1. Materials

Coal based AC was purchased from Shanxi Keling Co. Ltd. Zinc nitrate hexahydrate (AR, 99.0%), urea (AR, 99.0%) and ethanol absolute (AR, 99.7%) were obtained from Tianjin Kermel Chemical Reagent Co. Ltd. All the chemicals were used without further purification.

2.2. Preparation of the sorbents

Soft nitriding modifying AC matrix was carried out based on the reference [22] but with some modification. Typically, given amount of AC supports were physically ground and mixed with urea controlling the weight ratio of urea/AC at 0, 0.5, 1, respectively. The mixture was sealed in a crucible and then calcinated at 150 °C for 2 h and at 300 °C for another 2 h. The product was washed with deionized water and ethanol for 3 times and then dried at 60 °C for 4 h. The obtained *N*-modified AC support was further ground into 40–60 mesh particle and collected for use. The *N*-modified AC supports were denoted as *N*-AC-X, X is the weight ratio of urea/AC.

N-modified AC supported ZnO adsorbents were prepared as follows: 0.4 g of *N*-modified AC support was impregnated in 1 ml deionized aqueous containing 0.3657 g of $Zn(NO_3)_2{\cdot}6H_2O$ to pro-

duce sample containing 20 wt% ZnO. The obtained mixture was dried at 30 °C in oven for overnight to remove the solvent and then calcinated in N_2 atmosphere for 2 h at 300 °C. In addition, a series of sorbents were prepared using *N*-AC-0.5 as support by varying the ZnO loading content from 0 to 30 wt%, which could be tuned by varying the added weight of $Zn(NO_3)_2{\cdot}6H_2O$ The preparation process was the same as above mentioned. The fabricated sorbents were labelled as ZAN-X-Y, therein Z, A, N represented the ZnO, AC, and nitrogen, respectively. X referred to the weight ratio of urea/AC and Y was the wt% loadings of ZnO.

2.3. Characterization

The phase composition of the samples before and after desulfurization were detected on a Rigaku D/max-2500 diffractometer using Cu Kα radiation and the scan rate is 8°/min. The data between 5 and 80° was used for wide angle XRD studies. Textural properties were obtained by measuring the N_2 adsorption isotherms at −196 °C with a Quantachrome Autosorb iQ Station 1. Before measurement, samples were outgassed at 200 °C for 8 h. The surfaces area was calculated according to BrunauerEmmett-Teller (BET) method. Micropore volume was obtained from the *t*-plot method. DFT method was used to calculate the total pore volume and pore size distribution of the sorbents. The surface chemical states of elements was analyzed by X-ray photoelectron spectroscopy (XPS) on an AXIS Ultra DLD Spectrometer with Al K radiation. Transmission electron microscopy (TEM) images were collected on Tecnai G2F20 electron microscopy. Temperature-programmed desorption of CO_2 (CO_2-TPD) was operated in a fixed-bed continuous flow micro-reactor at atmospheric pressure. 0.1 g of sample was pretreated at 300 °C for 2 h in helium. After cooling down to 50 °C, the CO_2 was passed to the sample for 1 h. Then the TPD process was proceeded raising temperature from 50 to 300 °C with a heating rate of 10 °C min^{-1}.

2.4. Breakthrough tests

The H_2S removal performance of the sorbents was tested on a fixed bed by removing H_2S from a gas stream in moist N_2. Typically, the fabricated adsorbents were loaded into a U-tube micro-reactor (inner diameter 6 mm) with a packing height of 2 cm. Subsequently, the loaded sorbents was pre-humidified for 1.5 h using the moist N_2 (ca. 3% moisture), which obtained by bubbling N_2 in water at 30 °C. After that, the mixed gases containing H_2S, moist N_2 passed through the U-tube micro-reactor. The total flow rate was controlled at 100 ml/min. The inlet concentration of H_2S was 600 mg/m^3 and the reaction temperature was 30 °C. The inlet and outlet H_2S concentrations were determined by gas chromatograph equipped with a flame photometric detector (FPD). The breakthrough tests were stopped when the outlet concentration of H_2S reached 0.15 mg/m^3. The sulfur capacity of the sorbents was calculated by integrating the breakthrough curves area.

3. Results and discussion

3.1. Soft nitriding modification of activate carbon

The AC support before and after N functionalization using the soft nitriding technique are characterized by N_2 adsorption and XPS spectra, the results are shown in Fig. 1. The N_2 adsorption-desorption isotherms demonstrate that all the supports show type I sorption isotherms with a small H4 type hysteresis loop according to IUPAC classification. The inflection point appeared at relative pressures below 0.1 and the hysteresis loop emerged at relative pressure of 0.4 suggest the presence of micropores and mesopores in these supports [33]. Moreover, the amount of micropores account for a large proportion, because a steep rise of N_2 adsorption volume at $P/P^o < 0.1$ is found in all the material. Comparatively, the volume of N_2 uptake decrease in sequence of AC, *N*-AC-0.5 and *N*-AC-1, demonstrating a decrease of the surface area and porosity of the support after N modification.

The surface elemental composition of the supports were surveyed by XPS spectra, the results are shown in Fig. 1b. Apart from the peak of C1s, all supports depict the characteristic peak of O1s, indicating the presence of oxygen-containing species on their surface. Differently, a new peak corresponding to N1s is observed in *N*-AC-0.5 and *N*-AC-1 [34]. Both the N_2 adsorption and XPS spectra results strongly validate the successful incorporation of N species into AC matrix via soft nitriding technology. Moreover, the concentration of N species attached to AC surface can be controlled in a straightforward manner by changing the weight ratio of urea and AC.

3.2. Characterization of fresh sorbents

Fig. 2a shows the wide XRD pattern of AC, *N*-AC-0.5 and samples ZAN-X-20. Both AC and *N*-AC-0.5 show two obvious broad diffraction peaks at $2\theta = 28°$ and 43°, which attribute to the diffraction of (0 0 2) and (1 0 0) lattice planes of hexagonal graphite structure [35,36]. Nitrogen modification causes no obvious change to the XRD pattern compared with the pristine AC matrix. After supporting ZnO, these two broad diffraction peaks become weak, together with some new diffraction peaks corresponding to wurtzite structured ZnO [2] appeared. This indicates that zinc nitrates decompose to ZnO during the calcination and that the ZnO grains disperse well on the AC surface. Interestingly, the characteristic ZnO peaks intensify when supporting ZnO on N modified AC. Moreover, the peak intensity becomes even stronger with the increasing nitrogen content on the AC surface, illustrating that *N*-modified AC leads to the agglomeration of ZnO grains. This is thought to be caused by the decreased surface area of the *N*-modified AC support. In addition, varying the ZnO loading content on the *N*-AC-0.5 support can also lead to the variation of the ZnO diffraction peak intensity. The peaks intensify with increasing the ZnO loading content, just as shown in Fig. 2b.

In order to better understand the influence of *N*-modified AC on the dispersion and the grain size of ZnO nanoparticles, TEM characterization was performed. Fig. 3(a, d) firstly presents the images of AC support, which is a layer-like material composed of a disordered arrangement of nanosheets. After loading ZnO, the morphology of the support remains undistorted, and ZnO grains with irregular shapes are well dispersed onto the AC support (shown in Fig. 3(b, e)). Compared with ZAN-0-20, supporting ZnO grains on *N*-modified AC has no difference in morphology but influences the dispersion associated with the ZnO grains. Agglomeration of ZnO grains were observed according to Fig. 3(c, f), and are consistent with XRD results. Additionally, some mesoporous voids are observed in both samples loaded with ZnO because of the random packing of the carbon nanosheet or/and ZnO nanograins.

Fig. 4 shows the N_2 adsorption and desorption isotherms and the corresponding pore size distribution (PSD) curves of ZAN-0-20 and ZAN-0.5–20. For comparison, the N_2 adsorption results of pristine AC and *N*-AC-0.5 are also included. The results demonstrate that introducing ZnO into AC or *N*-AC-0.5 does not remarkably destroy their support framework structures, which continue to show type I sorption isotherms with a small H4 type hysteresis loop [37]. A significant decrease in N_2 adsorption volume compared to their bare support is observed due to the partial filling of the pore channels by nanosized ZnO grains. ZAN-0.5-20 presents a lower N_2 adsorption volume than that of ZAN-0-0.5, thus there is a lower surface area and porosity expressed in ZAN-0.5-20. The

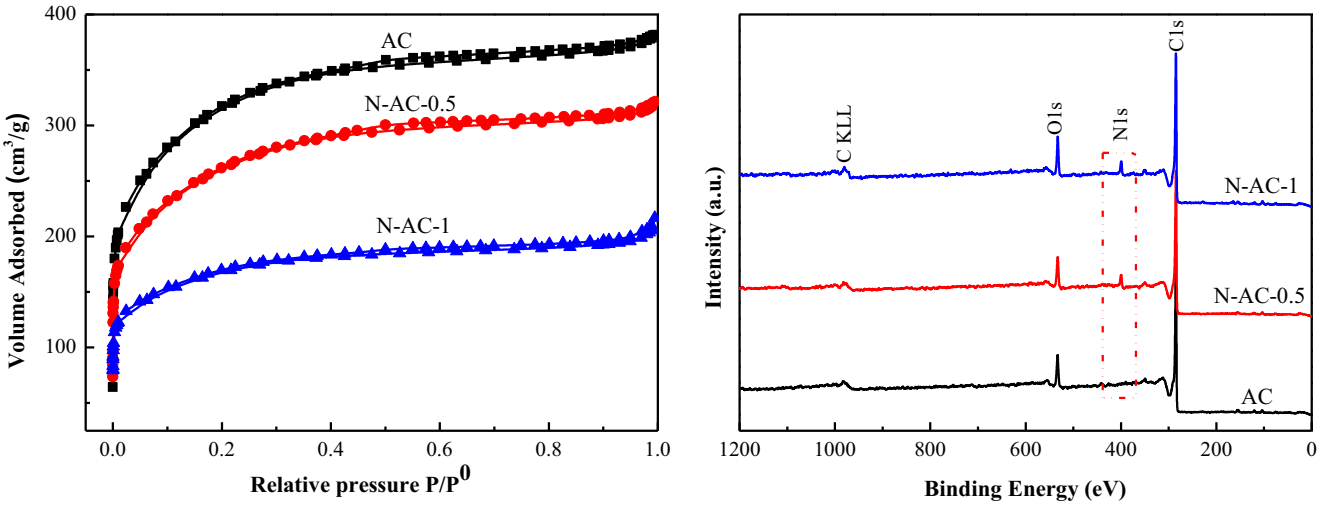

Fig. 1. N_2 adsorption and desorption isotherms (a) and the wide survey XPS spectra (b) of the supports.

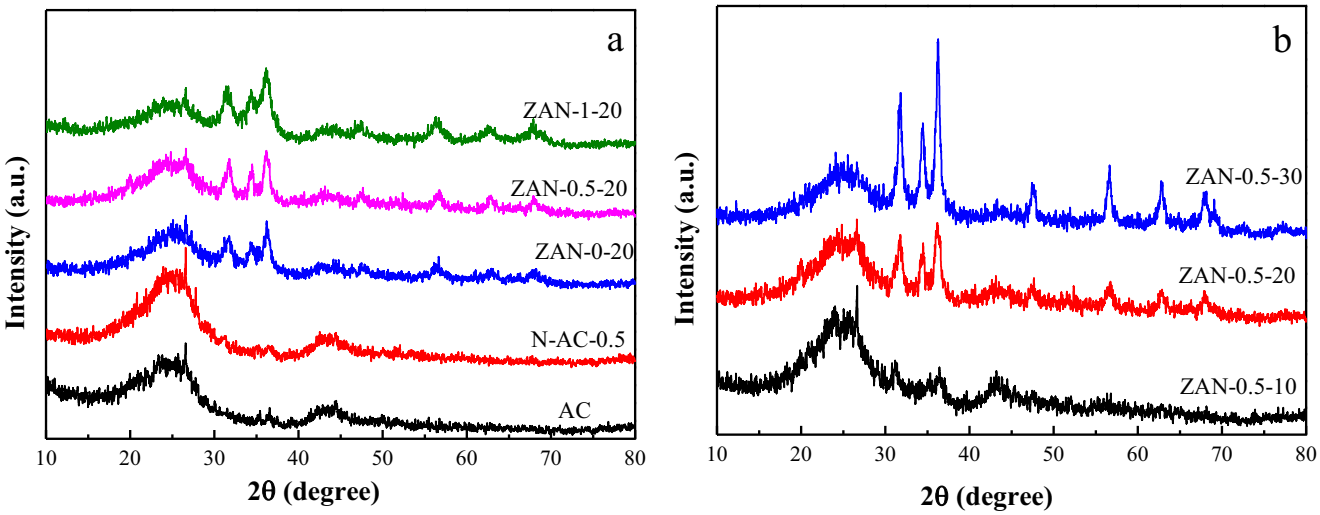

Fig. 2. XRD patterns of the support, ZAN-X-20 and ZAN-0.5-Y.

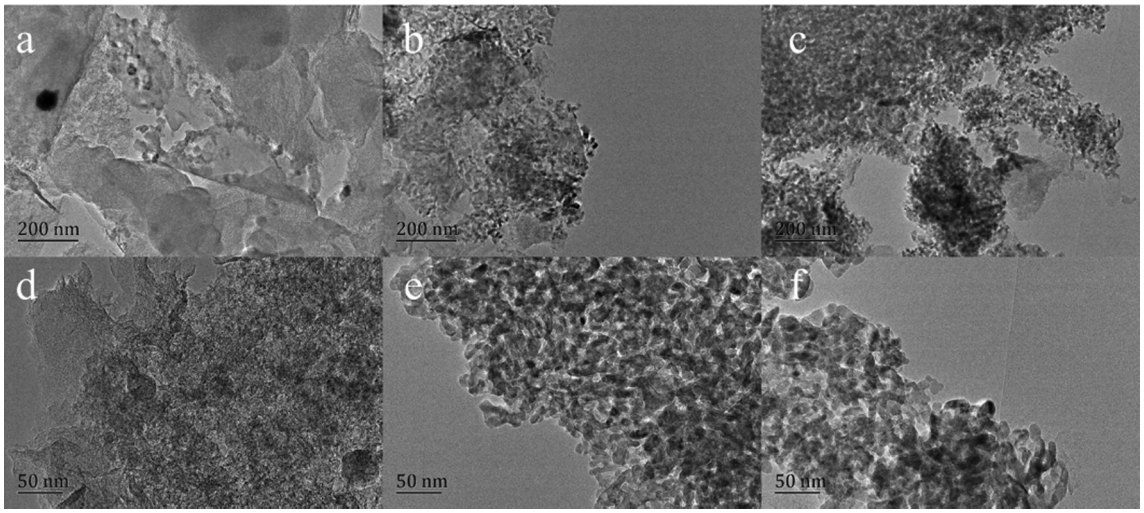

Fig. 3. TEM images of AC (a, d), ZAN-0-20 (b, e), ZAN-0.5-20 (c, f).

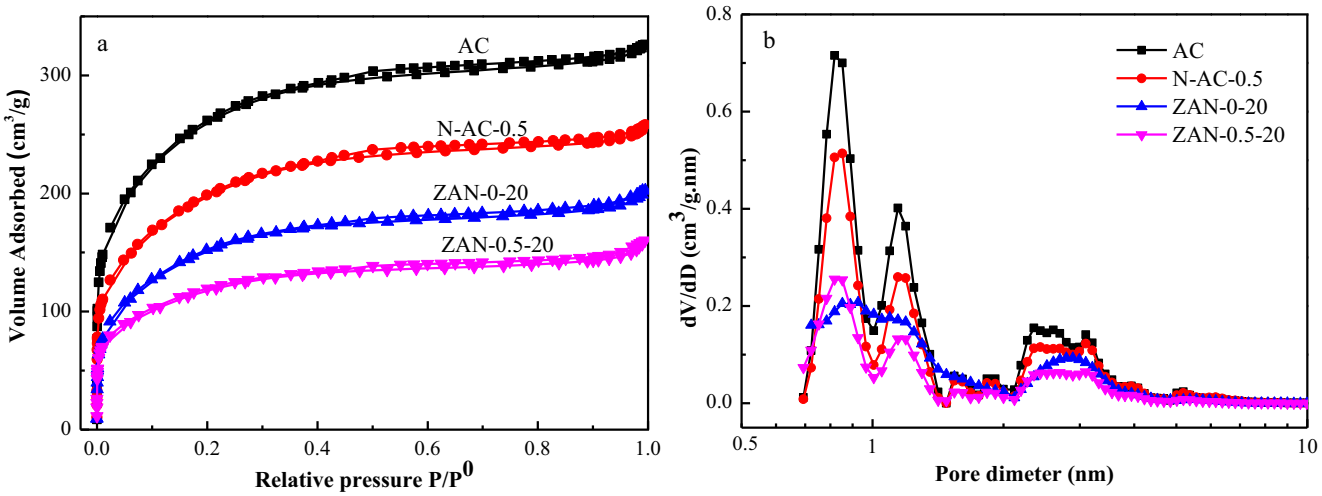

Fig. 4. N_2 adsorption and desorption isotherms (a) and the corresponded PSD (b) of the samples.

corresponding PSD curves suggest that all the samples have a tri-model PSD, which distributes at 0.8 nm, 1.3 nm and 3 nm. Supporting ZnO on AC or *N*-AC-0.5 causes the amount of micropores to decrease remarkably, consistent with findings from the N_2 adsorption results.

Table 1 shows the detailed texture parameters of the support and the fabricated samples. The pristine AC matrix takes a large surface area of 1119.8 m^2/g and pore volume of 0.59 cm^3/g, implying that the selected AC matrix is suitable for use as a support. *N*-modified AC (*N*-AC-0.5) exhibits decreased surface area and pore volume at 815.9 m^2/g and 0.45 cm^3/g, respectively. Dispersing ZnO nanoparticles on the support result in a significant decrease in their surface area and pore volume. Specifically, ZAN-0-20 has a surface area of 764.4 m^2/g and the total pore volume is 0.41 cm^3/g; ZAN-0.5-20 exhibits the corresponding values of 495.1 m^2/g and 0.28 cm^3/g, respectively. The decrease of surface are and pore volume suggest that the ZnO nanoparticles successfully occupy the pore channel of their support. This result is consistent with the N_2 adsorption isotherms.

The variation of the fabricated sorbents respect to ZnO-support interaction and surface characteristics before and after N modification are investigated by the XPS characterizations. Fig. 5 shows the Zn2p XPS spectra. As shown, the Zn 2p spectra of both samples show a doublet peaks with a binding energy gap of 23 eV, the doublet peaks are assigned to Zn2p3/2 and Zn2p1/2 lines with binding energies of 1022.5 eV and 1045.5 eV, respectively. These indicate the presence of a ZnO phase in both samples [38]. Zn 2p spectra of ZAN-0.5-20 displays a clear red shift in regard of binding energy compared with that of in ZAN-0-20. This suggests a decrease in electron density of ZnO in ZAN-0.5-20, highlighting the presence of interaction between ZnO and the *N*-modified AC support [9].

Fig. 5b displays high resolved O1s spectra of ZAN-0-20 and ZAN-0.5-20, illustrating the influence of N modification on the surface oxygen species of the adsorbents. Both of them are fitted into four components with binding energies of 531.2 ± 0.2 eV, 531.8 ± 0.1 eV, 532.6 ± 0.2 eV and 533.5 ± 0.3 eV. The former two peaks are ascribed to the lattice oxygen in ZnO [9] and the surface hydroxyl groups [3,9], respectively. The last two peaks are associated with the presence of sp^2 C—O bond [39,40] and the loosely bound oxygen species such as adsorbed O_2, or adsorbed H_2O on the surface [41,42]. Compared with ZAN-0-20, the ratio of surface hydroxyl groups accounting for total O in ZAN-0.5-20 shows an obvious increase (22.5% vs 19.9%), illustrating that *N*-functionalized AC support increases the basicity of the material. In addition, both samples have adsorbed oxygen accounting for 22–23% of the total O composition; this adsorbed oxygen can be used as oxidizer for catalytic oxidation of H_2S during desulfurization process.

Table 1
Physical properties of support and the as-prepared samples.

Sample	S_{BET} (m^2/g)	V_t (cm^3/g)	V_{mic} (cm^3/g)
AC	1119.8	0.59	0.34
N-AC-0.5	815.9	0.45	0.22
ZAN-0-20	764.4	0.41	0.24
ZAN-0.5-20	495.1	0.28	0.15

S_{BET}, BET specific area; V_t, total pore volume; V_{mic}, micropore volume.

The introduced N species have successfully changed the interaction between ZnO and AC matrix based on the results presented in Fig. 5a. However, the mechanism by which the introduced N species tune the interaction is unclear. In order to better understand this, the bonding configurations of the nitrogen species within the AC matrix before and after supporting ZnO are analyzed and shown in Fig. 5c, d. According to the XPS results, *N*-AC-0.5 has an atomic composition of 86.48% C, 4.61% N and 8.9% O. Generally, the introduced N atom has three bonding configurations within the carbon lattice, including graphitic N (or quaternary N), pyridinic N, and pyrrolic N [43]. Herein, a large percentage of N atoms (64.8%) possessing a binding energy of 400 eV, are indexed to amine and amide groups (or pyrrolic N) [22,32]. The peak positioned at 401.1 eV is attributed to graphitic N (8.3%) that replaced carbon atoms in the hexagonal ring [30,44]. The peak centered at 398.7 eV is assigned to the pyridine N (26.9%) [43,45]. After supporting ZnO, the atomic composition changed into 75.8% C, 2.34% N, 15.08% O and 6.79% Zn. In comparison to *N*-AC-0.5, the number of surface N atoms in ZAN-0.5-20 dramatically decreased, which is interpreted by the coverage of ZnO nanoparticles. In addition, although the category of nitrogen atoms is unvaried, the percentage remarkably changes. The percentage of pyrrolic N decreases from 64.8% to 43.8%, while the percentage of pyridine N and the graphitic N increase to 43.2% and 13.0%, respectively. These information imply that partial pyrrolic N converts to pyridine N and graphitic N after supporting ZnO onto *N*-modified AC; this is thought to be a result of the deprotonation of amine and amide groups which occur during thermal decomposition of zinc nitrates, resulting in the conversion of pyrrolic N to pyridine N or graphite N. Such a conversion at a mild temperature was also found by other groups [46,47].

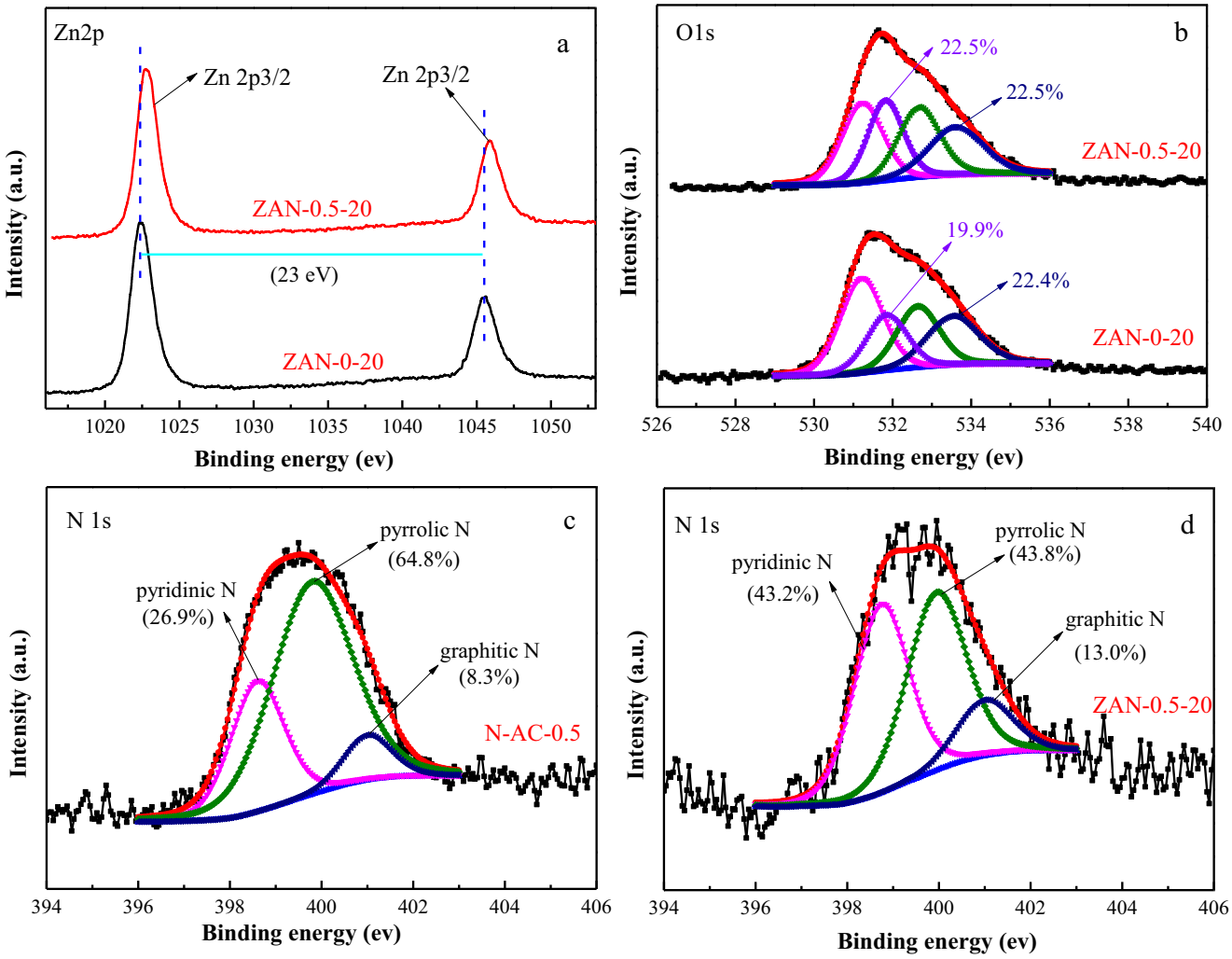

Fig. 5. XPS spectra of Zn2p (a), O1s (b), N1s (c, d) for the selected samples.

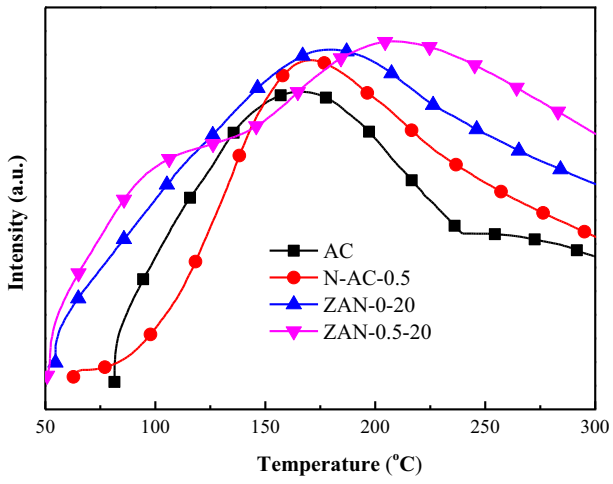

Fig. 6. CO_2-TPD curves of the supports and their corresponding samples.

The influence of N modification on the basicity of supports and their corresponding samples are recorded by CO_2-TPD curves in Fig. 6. Both the supports and samples exhibit a broad CO_2 desorption peak ranged from 100 °C to 300 °C. As known, CO_2 desorption volume of the material positively relies on the surface area and the amount of surface basic groups [48]. In terms of these two supports (AC and *N*-AC-0.5), the virgin AC matrix has a larger surface area but shows a lower CO_2 adsorption volume, suggesting that the surface basicity of the AC is enhanced after introducing N species (including pyrrolic N, pyridine N and graphitic N). The enhanced surface basicity is related to the introduced N species, which provide basic sites for interacting with CO_2 [48]. It is noted that the desorbed CO_2 from the virgin AC is attributed to physically adsorbed CO_2 on the AC surface; the unique micro-porosity leads to a high desorbed temperature. Introducing ZnO nanoparticles on pristine AC and *N*-AC-0.5 resulted in an further improved surface basicity, which is attributed to the surface hydroxyl formed by the hydroxylation of ZnO [3]; this is confirmed by the release of a larger CO_2 desorption volume observed from their CO_2-TPD curves. The surface basicity of the supports and the samples vary in order of largest to smallest as: ZAN-0.5-20, ZAN-0-20, *N*-AC-0.5, AC. In brief, N modification significantly increases the amount of basic sites both in support and in the samples, which aids in the dissociation of H_2S.

3.3. Evaluation of H_2S removal performance

Fig. 7a shows the breakthrough curves of ZAN-X-20 series. For comparison, the breakthrough curves of virgin AC and *N*-AC-0.5 are also included. Clearly, the AC matrix has an ignored H_2S

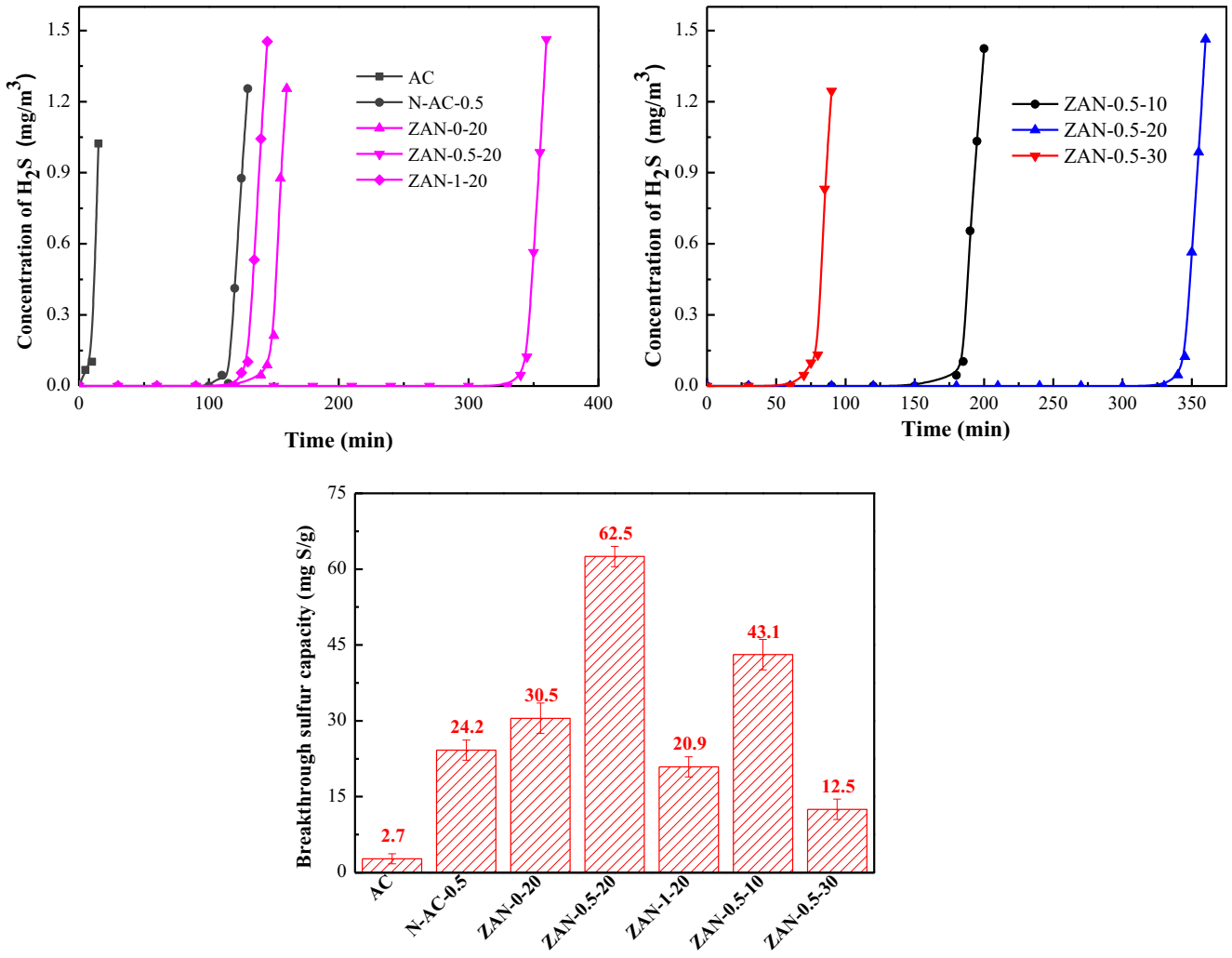

Fig. 7. Breakthrough curves of samples ZAN-X-20 (a), ZAN-0.5-Y (b) and the corresponding BSC (c).

removal capacity while the *N*-AC-0.5 expresses a breakthrough time of 105 min. This clearly demonstrates that *N*-modified AC contributes to the H_2S removal. In respect to ZAN-X-20 sorbents, the breakthrough time of the samples prolongs from 150 min (ZAN-0-20) to 345 min (ZAN-0.5-20) and then drastically decreases to 120 min (ZAN-1-20) with increasing concentration of N atoms on the AC matrix. As presented in Fig. 7c, ZAN-0-20, ZAN-0.5–20 and ZAN-1-20 show a BSC of 30.5, 62.5 and 20.9 mg S/g sorbent, respectively. The reduced H_2S uptake ability of ZAN-1-20 is caused by the introduced high concentration of N atoms that remarkably reduces the specific surface area and the pore volume of the support. This results in the agglomeration of ZnO grains and leads to a decrease in H_2S uptake ability.

Fig. 7b shows the H_2S removal performance of sorbents ZAN-0.5-Y. With an increase of the ZnO loading content from 0 to 30 wt%, the H_2S removal performance of the sorbents ZAN-0.5-Y also presents a volcano type variation, thus ZAN-0.5–20 is the best candidate for H_2S removal. Compared with *N*-AC-0.5 (24.2 mg S/g sorbent), ZAN-0.5-10 (43.1 mg S/g sorbent) and ZAN-0.5-20 (62.5 mg S/g sorbent) take an enlarged sulfur capacity, moreover their values are larger than that of ZAN-0-20 (30.5 mg S/g sorbent). This highlights the presence of synergistic effect between ZnO and N modified AC support during desulfurization. In regards to sorbents ZAN-0.5-Y, the amount of active sites initially increases with an increased ZnO loading content, however, an excessive increase will cause an aggregation of ZnO grains that results in a reduction of the active sites and porosity [49], thus the sulfur capacity of the sorbent decreases.

Table 2 summaries the performance of supported ZnO adsorbents to remove hydrogen sulfide at room temperature. The sorbents with different types of support such as mesoporous sieves, AC, and graphite oxide are included. As is seen, ZAN-0-20 shows a similar BSC compared with the sorbents reported in the references; however, ZAN-0.5-20 takes a higher BSC than most of the other supports, demonstrating the high efficiency of this strategy.

3.4. Analysis of the sulfide products

According to the characterization and breakthrough results from fresh samples, although ZAN-0-20 and ZAN-0.5-20 show some similar characteristics (such as ZnO loading content, ZnO grain size and the dispersion), ZAN-0.5-20 possesses a BSC (62.5 mg S/g sorbent) two times larger than that of ZAN-0-20 (30.5 mg S/g sorbent). To clearly illustrate the contributors for boosting a robust H_2S uptake on the sample ZAN-0.5-20, the spent samples ZAN-0-20E and ZAN-0.5-20E were characterized.

Fig. 8a shows the XRD pattern of the sulfided samples. Clearly, the diffraction peaks of graphite structure at $2\theta = 28^\circ$ is still retained, suggesting the desulfurization process does not damage the support structure. Compared with the fresh samples, the

Table 2
Summary of BSC of supported ZnO based adsorbents at room temperature.

Samples	C_{out} (H_2S) (ppm)	Loadings (wt%)	BSCs (mg S/g sorbent)	Reference
ZnBW	100		12.5	[24]
$Cu_{0.5}Zn_{0.5}$/AC	60	10	27.2	[14]
TRGZ-3	15	50	114	[50]
Z30/K6	0.1	30	37.6	[4]
M-Z20/M41	0.1	30	54.9	[13]
ZAN-0-20	0.1	20	30.5	In this work
ZAN-0.5-20	0.1	20	62.5	In this work

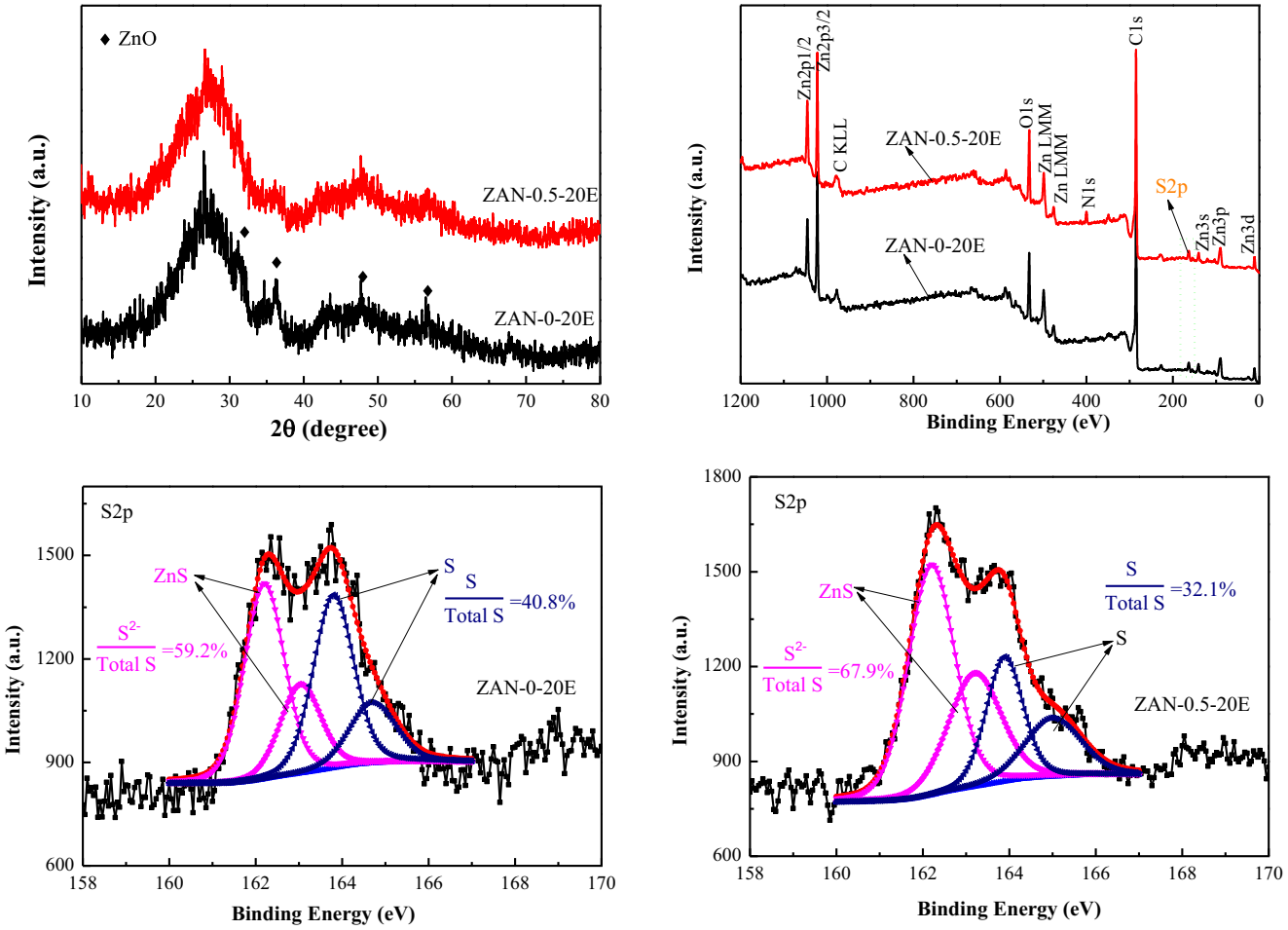

Fig. 8. XRD pattern (a), the wide survey scan of the XPS spectra (b), and S2p XPS spectra of the spent adsorbents.

characteristic peaks of ZnO become weakened but still appreciable in ZAN-0-20E. In contrast, the characteristic peaks in ZAN-0.5-20E almost disappear, indicating the low reactivity of ZnO toward H_2S in ZAN-0-20. Additionally, although a large amount of H_2S was adsorbed by these two sorbents, no signal peaks related to sulfur species, such as ZnS or/and elemental sulfur, are found in their XRD patterns.

XPS characterizations are further performed to distinguish the formed sulfur species in the spent samples. Fig. 8b shows the wide survey scan XPS spectra of these two spent samples, in which the signal peak of S2p are found in both samples. Based on the high resolution XPS spectrum of S2p shown in Fig. 8c, d, the doublet peaks located at ca. 162.0 ± 0.2 eV and 163.1 ± 0.2 eV are attributed to S species in ZnS. These two peaks correspond to the spin orbit splitting of S2p3/2 and S2p1/2 in ZnS, respectively [51]. While the doublet peaks positioned at ca. 163.7 ± 0.2 eV and 164.8 ± 0.2 eV are assigned to elemental sulfur [52]. Therein, the formed S^{2-} in ZnS accounts for 59.2% of total S in ZAN-0-20E and 67.9% in ZAN-0.5-20E, respectively. Therefore, it concludes that the main component of the sulfide products are ZnS and elemental sulfur in both samples.

3.5. Adsorption mechanism of the sorbents with and without N modification

Based on the results from Fig. 8, ZnS and elemental sulfur are the products of these two adsorbents after desulfurization, suggesting that the desulfurization process includes chemical adsorption and catalytic oxidation. As mentioned, the dynamic breakthrough tests in this study were performed under an anaerobic condition, the oxygen containing groups or/and the adsorbed oxygen on the surface of AC matrix are inferred to act as an oxidizer for oxidizing H_2S to elemental S. The pristine AC matrix shows negligible H_2S uptake capacity, not only demonstrating that

the physical adsorption of H_2S by the sorbents is negligible, but also indicating that a driven force is required for catalytic oxidation of H_2S. As reported, alkali (such as MgO, Na_2CO_3, nitrogen containing species) modified AC is usually used as catalyst for catalytic oxidation of H_2S to elemental sulfur under wet conditions. The alkali salts improve the basicity of the water film condensed on the surface of AC, beneficial for H_2S dissociation [25,30,53,54]. Therefore, we can surmise the sulfidation process in ZAN-0-20 is that the water vaper in the feedstock firstly condensates as a water film on the sorbent surface. Then hydroxylation occurs on the surface of ZnO nano-grains, which provides a weak alkali environment [3,49]; the molecular H_2S diffused to the water film to dissociate into HS^- or S^{2-}. Eventually the dissociated HS^- and S^{2-} are oxidized into elemental S by the adsorbed oxygen species on the AC surface [55]. In addition, the dissociated HS^- and S^{2-} can also react with ZnO to form ZnS.

Whereas in ZAN-0.5-20, aside from the hydroxylated ZnO nanograins, the introduced N species (including pyrrolic N, pyridine N and graphitic N) attached to AC surface can also increase the local basicity of the water film, further facilitating the dissociation of H_2S. Similar results were concluded in previous studies [25,27,56,57]. Because the dissociation of H_2S into HS^- is the rate determining step for catalytic oxidation of H_2S [53], thus the higher concentrations of HS^- will generate more elemental S by oxidation. In addition, the introduced N species can also participate in the oxidation of H_2S [58].This is further validated by the breakthrough results of AC and *N*-AC-0.5, where AC has a sulfur capacity of 2.7 mg S/g sorbent while the *N*-AC-0.5 is 24.2 mg S/g sorbent.

Table 3 provides the surface atomic concentrations of ZAN-0-20 and ZAN-0.5-20 before and after desulfurization based on the XPS results. As seen, the atomic concentrations of C, Zn, N of these two samples before and after desulfurization have no obvious change, while the atomic concentrations of O decreases. ZAN-0.5-20E (3.36%) shows the atomic concentration of sulfur is higher than that of ZAN-0-20E (2.24%), indicating ZAN-0.5-20 adsorbs more H_2S during desulfurization process, this is consistent with the breakthrough results. Notably, these detected values by XPS characterization, which only reflect the surface information of the sorbents, are much lower than their actual BSC. This suggests that the reaction between H_2S and ZnO in these sorbents also permeates in the bulk of ZnO [59]. Hence, the rate of lattice diffusion plays an important role in enhancing the BSC of the sorbents. Because the characteristic peaks of ZnO completely disappeared in ZAN-0.5-20E while remaining appreciable in ZAN-0-20E, it is concluded that more ZnO in ZAN-0.5-20 participates in the reaction with H_2S. This provides further evidence that ZAN-0.5-20 has a faster lattice diffusion rate. As aforementioned, the interaction between ZnO and the *N*-modified AC lead to a decrease of electron density of ZnO, which can induce the generation of some defect sites, such as oxygen vacancies and grain boundaries [60]. These defective sites are believed to promote the lattice diffusion. In addition, the higher concentrations HS^- or S^{2-} in the water film in ZAN-0.5-20 will also contribute to the fast lattice diffusion.

As discussed above, the water vapor in the feedstocks, which firstly condensate as water film on the adsorbent surface, and then catalyze the dissociation of H_2S into HS^- or/and S^{2-}, is very important for improving H_2S uptake capacity. The positive role of water on H_2S removal was tested by the breakthrough experiment carried out in dry conditions, as shown in Fig. 9. Both ZAN-0-20 and ZAN-0.5-20 show a lower BSC at dry conditions than those operated in wet conditions. The lower BSC of the sorbents in dry conditions, besides the catalytic effect of water, maybe also relate to the solvation of ZnO in the water film [61].

Table 3
The atomic composition in ZAN-0-20 and ZAN-0.5-20 before and after desulfurization.

Sample	C (%)	O (%)	Zn (%)	N (%)	S (%)
ZAN-0-20	78.81	14.08	7.11	0	0
ZAN-0-20E	78.42	12	7.24	0	2.24
ZAN-0.5-20	75.8	15.08	6.79	2.34	0
ZAN-0.5-20E	75.61	11.33	6.72	2.98	3.36

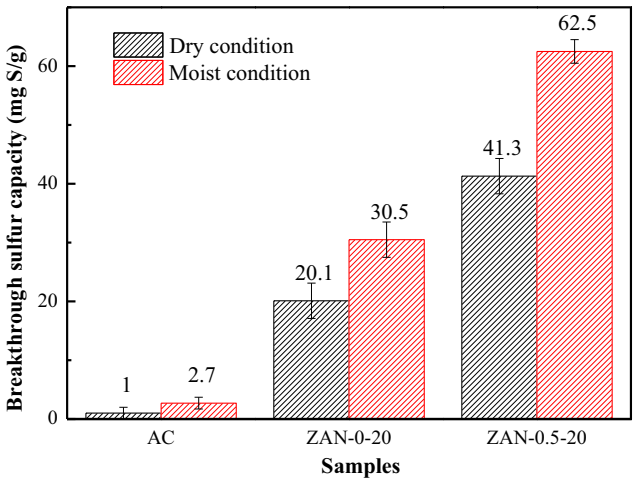

Fig. 9. H_2S removal performance of the sorbents in dry and wet conditions.

In brief, the enhanced BSC in ZAN-0.5-20 compared with ZAN-0-20 is attributed to the introduced nitrogen species on the AC surface, which not only serve as basic sites that increase the basicity of the water film in the pores and promotes the dissociation of H_2S and H_2O, but also can produce an electron defective state of ZnO that accelerates the rate of lattice diffusion. In addition, water vapor in the feedstock also plays a positive effect on H_2S removal. These results validate the effectiveness of our strategy: tuning the pore acid-basic environment and the interaction between the support and active sites to boost a robust H_2S uptake over the fabricated sorbents.

4. Conclusion

A series of highly efficient N modified AC supported ZnO adsorbents were prepared by tuning the ZnO-AC interaction via introducing N species on AC surface. The nitrogen content attached onto the AC surface was controlled by modulating the weight ratio of urea/AC. H_2S breakthrough results indicated that *N*-modified AC with ZnO as an adsorbent could significantly improve the H_2S removal capacity. The maximum BSC of the fabricated samples was 62.5 mg S/g sorbent, two times larger than that sorbent without *N*-modification. The enhanced BSC was attributed to the introduced nitrogen species, which not only served as basic sites, but also increased the basicity of the water film in the pores, promoting the dissociation of H_2S and H_2O, while also modifying the electronic structure of ZnO, resulting in an acceleration of the rate of lattice diffusion. In addition, it was found that the high BSC of the sorbent was also related to the doped N concentrations, ZnO dispersion and the material porosity.

Further improvement on using the different types of AC as a support could be made in order to examine the versatility of this new strategy.

Acknowledgements

This work is financially supported by the Key Projects of National Natural Science Foundation of China (Grant No.

21736007) and the National Natural Science Foundation of China (Grant No. 21576180 and 21878209).

References

[1] P.R. Westmoreland, Evaluation of candidate solids for high-temperature desulfurization of low-Btu gases, Environ. Sci. Technol. 10 (1976) 659–661.
[2] C. Yang, J. Wang, H. Fan, Y. Hu, Activated carbon-assisted fabrication of cost-efficient ZnO/SiO_2 desulfurizer with characteristic of high loadings and high dispersion, Energy Fuel. 32 (2018) 6064–6072.
[3] C. Yang, J. Wang, H.-L. Fan, Contributions of tailored oxygen vacancies in ZnO/Al_2O_3 composites to the enhanced ability for H_2S removal at room temperature, Fuel 215 (2018) 695–703.
[4] L. Li, T.H. Sun, C.H. Shu, Low temperature H_2S removal with 3-D structural mesoporous molecular sieves supported ZnO from gas stream, J. Hazard Mater. 311 (2016) 142–150.
[5] H. Xia, B. Liu, High H_2O-resistance CaO-MnOx/MSU-H sorbents for hot coal gas desulfurization, J. Hazard Mater. 324 (2017) 281–290.
[6] H.F. Garces, H.M. Galindo, L.J. Garces, Low temperature H_2S dry-desulfurization with zinc oxide, Micropor. Mesopor. Mater. 127 (2010) 190–197.
[7] M. Mureddu, I. Ferino, A. Musinu, MeO_x/SBA-15 (Me = Zn, Fe): highly efficient nanosorbents for mid-temperature H_2S removal, J. Mater. Chem. A. 2 (2014) 19396–19406.
[8] B. Bajaj, H.-I. Joh, S.M. Jo, Enhanced reactive H_2S adsorption using carbon nanofibers supported with Cu/Cu_xO nanoparticles, Appl. Surf. Sci. 429 (2018) 253–257.
[9] H.S. Song, M.G. Park, W. Ahn, Enhanced adsorption of hydrogen sulfide and regeneration ability on the composites of zinc oxide with reduced graphite oxide, Chem. Eng. J. 253 (2014) 264–273.
[10] Y. He, Y. Wang, L. Zhang, High-efficiency conversion of CO_2 to fuel over ZnO/g-C_3N_4 photocatalyst, Appl. Catal. B 168–169 (2015) 1–8.
[11] R. Portela, F. Rubio-Marcos, Nanostructured ZnO/sepiolite monolithic sorbents for H_2S removal, J. Mater. Chem. A 3 (2014) 1306–1316.
[12] M. Hussain, N. Abbas, Novel mesoporous silica supported ZnO adsorbents for the desulphurization of biogas at low temperatures, Chem. Eng. J. 188 (2012) 222–232.
[13] Q. Geng, L.J. Wang, C. Yang, Room-temperature hydrogen sulfide removal with zinc oxide nanoparticle/molecular sieve prepared by melt infiltration, Fuel Process. Technol. 185 (2019) 26–37.
[14] M. Balsamo, S. Cimino, ZnO-CuO supported on activated carbon for H_2S removal at room temperature, Chem. Eng. J. 304 (2016) 399–407.
[15] G. de Falco, F. Montagnaro, M. Balsamo, Synergic effect of Zn and Cu oxides dispersed on activated carbon during reactive adsorption of H_2S at room temperature, Micropor. Mesopor. Mater. 257 (2018) 135–146.
[16] J.C. Matsubu, S. Zhang, L. Derita, Adsorbate-mediated strong metal–support interactions in oxide-supported Rh catalysts, Nat. Chem. 9 (2017) 120–127.
[17] L. Thomas, S. Julia, Formation of a ZnO overlayer in industrial Cu/ZnO/Al_2O_3 catalysts induced by strong metal-support interactions, Angew. Chem. Int. Ed. 54 (2015) 4544–4548.
[18] O. Mabayoje, M. Seredych, Cobalt (hydr)oxide/graphite oxide composites: importance of surface chemical heterogeneity for reactive adsorption of hydrogen sulfide, J. Colloid Interf. Sci. 378 (2012) 1–9.
[19] S. Mykola, M. Oluwaniyi, Visible-light-enhanced interactions of hydrogen sulfide with composites of zinc (oxy)hydroxide with graphite oxide and graphene, Langmuir 28 (2012) 1337–1346.
[20] S. Cimino, L. Lisi, Highlighting the effect of the support during H_2S adsorption at low temperature over composite Zn-Cu sorbents, Fuel 221 (2018) 374–379.
[21] R. Ullah, Z. Zhang, P. Bai, One-pot cation–anion double hydrolysis derived Ni/ZnO–Al_2O_3 absorbent for reactive adsorption desulfurization, Ind. Eng. Chem. Res. 55 (2016) 3751–3758.
[22] B. Liu, H. Yao, W. Song, Ligand-free noble metal nanocluster catalysts on carbon supports via "soft" nitriding, J. Am. Chem. Soc. 138 (2016) 4718–4721.
[23] Y. Li, X. Liu, Activated carbon/ZnO composites prepared using hydrochars as intermediate and their electrochemical performance in supercapacitor, Mater. Chem. Phys. 148 (2014) 380–386.
[24] D. Nguyen-Thanh, T.J. Bandosz, Activated carbons with metal containing bentonite binders as adsorbents of hydrogen sulfide, Carbon 43 (2005) 359–367.
[25] F. Sun, J. Liu, H. Chen, Nitrogen-rich mesoporous carbons: highly fficient, regenerable metal-free catalysts for low-temperature oxidation of H_2S, ACS Catal. 3 (2013) 862–870.
[26] A. Bagreev, J.A. Menendez, I. Dukhno, Bituminous coal-based activated carbons modified with nitrogen as adsorbents of hydrogen sulfide, Carbon 42 (2004) 469–476.
[27] Z. Yu, X. Wang, Molten salt synthesis of nitrogen-doped porous carbons for hydrogen sulfide adsorptive removal, Carbon 95 (2015). S0008622315301226.
[28] V.Z. Radkevich, T.L. Senko, The influence of surface functionalization of activated carbon on palladium dispersion and catalytic activity in hydrogen oxidation, Appl. Catal. A 335 (2012) 241–251.
[29] M. Abdouss, N. Hazrati, Effect of the structure of the support and the aminosilane type on the adsorption of H_2S from model gas, RSC Adv. 4 (2014) 6337.
[30] Z. Yu, X. Wang, Nitrogen-doped mesoporous carbon nanosheets derived from metal-organic frameworks in a molten salt medium for efficient desulfurization, Carbon 117 (2017) 376–382.
[31] W. Shen, W. Fan, Nitrogen-containing porous carbons: synthesis and application, J. Mater. Chem. A. 1 (2013) 999–1013.
[32] J. Lei, B. Liu, W. Pu, H. Yao, Ultrasmall Au nanocatalysts supported on nitrided carbon for electrocatalytic CO_2 reduction: the role of the carbon support in high selectivity, Nanoscale (2018).
[33] R.H. Shi, Z.R. Zhang, H.L. Fan, Cu-based metal–organic framework/activated carbon composites for sulfur compounds removal, Appl. Surf. Sci. 394 (2017) 394–402.
[34] X. Ma, H. Li, T. Liu, Comparison of photocatalytic reaction-induced selective corrosion with photocorrosion: impact on morphology and stability of Ag-ZnO, Appl. Catal. B 201 (2017) 348–358.
[35] D. Zhu, J. Jiang, A general strategy to synthesize high-level N-doped porous carbons: via Schiff-base chemistry for supercapacitors, J. Mater. Chem. A 6 (2018).
[36] T. Wang, S. Tan, C. Liang, Preparation and characterization of activated carbon from wood microwave-induced ZnCl activation, Carbon 47 (2009) 1880–1883.
[37] M. Thommes, K. Kaneko, Physisorption of gases, with special reference to the evaluation of surface area and pore size distribution (IUPAC Technical Report), Pure Appl. Chem. 87 (2015) 1051–1069.
[38] D.K. Mishra, J. Mohapatra, Carbon doped ZnO: Synthesis, characterization and interpretation, J. Magn. Magn. Mater. 329 (2013) 146–152.
[39] C.D. Zangmeister, Preparation and evaluation of graphite oxide reduced at 220 °C, Chem. Mater. 22 (2010) 5625–5629.
[40] Y.J. Xu, G. Weinberg, Nanoarchitecturing of activated carbon: facile strategy for chemical functionalization of the surface of activated carbon, Adv. Funct. Mater. 18 (2008) 3613–3619.
[41] S. Feliu, V. Barranco, XPS study of the surface chemistry of conventional hot-dip galvanised pure Zn, galvanneal and Zn–Al alloy coatings on steel, Acta Mater. 51 (2003) 5413–5424.
[42] E.D.L. Rosa, S. Sepúlveda-Guzman, Controlling the growth and luminescence properties of well-faceted ZnO nanorods, J. Phys. Chem. C 111 (2007) 8489–8495.
[43] H. Wang, T. Maiyalagan, X. Wang, Review on recent progress in nitrogen-doped graphene: synthesis, characterization, and its potential applications, ACS Catal. 2 (2012) 781–794.
[44] Z. Yu, X. Wang, Molten salt synthesis of nitrogen-doped porous carbons for hydrogen sulfide adsorptive removal, Carbon 95 (2015) 852–860.
[45] D. Zhu, J. Jiang, D. Sun, A general strategy to synthesize high-level N-doped porous carbons via Schiff-base chemistry for supercapacitors, J. Mater. Chem. A 6 (2018) 12334–12343.
[46] Q. Zhu, S.L. Money, Determination of the fate of nitrogen functionality in carbonaceous materials during pyrolysis and combustion using X-ray absorption near edge structure spectroscopy, Langmuir 13 (1997) 2149–2157.
[47] J.R. Pels, F. Kapteijn, Evolution of nitrogen functionalities in carbonaceous materials during pyrolysis, Carbon 11 (1995) 1641–1653.
[48] W. Shen, S. Zhang, Y. He, Hierarchical porous polyacrylonitrile-based activated carbon fibers for CO_2 capture, J. Mater. Chem. 21 (2011) 14036.
[49] L.J. Wang, H.L. Fan, Design of a sorbent to enhance reactive adsorption of hydrogen sulfide, ACS Appl. Mater. Interf. 6 (2014) 21167–21177.
[50] S.P. Lonkar, V. Pillai, In situ formed graphene/ZnO nanostructured composites for low temperature hydrogen sulfide removal from natural gas, RSC Adv. 6 (2016) 81142–81150.
[51] R. Zhang, Y. Wang, One-pot hydrothermal synthesis of ZnS quantum dots/graphene hybrids as a dual anode for sodium ion and lithium ion batteries, Appl. Surf. Sci. 437 (2018) 375–383.
[52] X. Hao, Y. Wang, Zinc vacancy-promoted photocatalytic activity and photostability of ZnS for efficient visible-light-driven hydrogen evolution, Appl. Catal. B 221 (2018) 302–311.
[53] Z. Zhang, J. Wang, W. Li, Millimeter-sized mesoporous carbon spheres for highly efficient catalytic oxidation of hydrogen sulfide at room temperature, Carbon 96 (2016) 608–615.
[54] A. Bagreev, J. Angel Menendez, Bituminous coal-based activated carbons modified with nitrogen as adsorbents of hydrogen sulfide, Carbon 42 (2004) 469–476.
[55] D.V. Brazhnyk, Y.P. Zaitsev, Oxidation of H_2S on activated carbon KAU and influence of the surface state, Appl. Catal. B 70 (2007) 557–566.
[56] X. Kan, X. Chen, W. Chen, Nitrogen-decorated, ordered mesoporous carbon spheres as high-efficient catalysts for selective capture and oxidation of H_2S, ACS Sustain. Chem. Eng. 7 (2019) 7609–7618.
[57] S. Bashkova, F.S. Baker, Activated carbon catalyst for selective oxidation of hydrogen sulphide: on the influence of pore structure, surface characteristics, and catalytically-active nitrogen, Carbon 45 (2007) 1354–1363.
[58] M. Seredych, T.J. Bandosz, Role of microporosity and nitrogen functionality on the surface of activated carbon in the process of desulfurization of digester gas, J. Phys. Chem. C. 12 (2008) 4704–4711.
[59] G. Liu, Z.H. Huang, F. Kang, Preparation of ZnO/SiO_2 gel composites and their performance of H_2S removal at room temperature, J. Hazard Mater. 215–216 (2012) 166–172.
[60] M.D. McCluskey, S.J. Jokela, Defects in ZnO, J. Appl. Phys. 106 (2009) 071101.
[61] D.A. Giannakoudakis, Highly efficient air desulfurization on self-assembled bundles of copper hydroxide nanorods, ACS Appl. Mater. Interf. 8 (2016) 31986–31994.